Fractional Calculus and Applied Analysis (2022) 25:1801–1817
https://doi.org/10.1007/s13540-022-00081-9

ORIGINAL PAPER

Optimized fractional-order Butterworth filter design in complex *F*-plane

Shibendu Mahata[1] · **Norbert Herencsar**[2] · **David Kubanek**[2] · **I. Cem Goknar**[3]

Received: 26 March 2022 / Revised: 2 August 2022 / Accepted: 2 August 2022 /
Published online: 15 September 2022

Abstract

This paper introduces a new technique to optimally design the fractional-order Butterworth low-pass filter in the complex F-plane. Design stability is assured by incorporating the critical phase angle as an inequality constraint. The poles of the proposed approximants reside on the unit circle in the stable region of the F-plane. The improved accuracy of the suggested scheme as compared to the recently published literature is demonstrated. A mixed-integer genetic algorithm which considers the parallel combinations of resistors and capacitors for the Valsa network is used to optimize the frequency responses of the fractional-order capacitor emulators as part of the experimental verification using the Sallen–Key filter topology. The total harmonic distortion and spurious-free dynamic range of the practical 1.5th-order Butterwoth filter are measured as 0.13% and 62.18 dBc, respectively; the maximum and mean absolute relative magnitude errors are 0.03929 and 0.02051, respectively.

✉ David Kubanek
kubanek@vut.cz

Shibendu Mahata
shibendu.mahata@bcrec.ac.in

Norbert Herencsar
herencsn@vut.cz

I. Cem Goknar
cem.goknar@isikun.edu.tr

[1] Department of Electrical Engineering, Dr. B. C. Roy Engineering College, Durgapur, West Bengal 713206, India

[2] Department of Telecommunications, Faculty of Electrical Engineering and Communication, Brno University of Technology, Technicka 12, 616 00 Brno, Czech Republic

[3] Department of Electrical and Electronics Engineering, Isik University, University Str. 2, 34980 Sile, Istanbul, Turkey

Keywords Fractional-order system (primary) · Analog filter approximation · F-domain · Fractional-order capacitor · Constrained optimization · Fractional-order Butterworth filter · Stability

Mathematics Subject Classification 26A33 (primary)93B50 · 93C99 · 93E11

1 Introduction

The Riemann–Liouville definition for the fractional derivative of arbitrary order υ for a function $f(t)$ is given by

$$ {}_aD_t^{\upsilon} f(t) = \frac{1}{\Gamma(n-\upsilon)} \frac{d^n}{dt^n} \int_a^t (t-\tau)^{n-\upsilon-1} f(\tau) d\tau, \tag{1} $$

where $n \in Z^+$; $n-1 < \upsilon \leq n$; a and t are the limits of the operation; and $\Gamma(\cdot)$ denotes the gamma function [13, 20, 23]. For zero initial conditions, the Laplace transform of (1) is given by $s^{\upsilon} F(s)$.

Applications of fractional calculus are pervading in various engineering disciplines [15], including fractional-order (FO) circuit theory and filter design [19]. Due to the presence of additional design parameters or 'tuning knobs' (viz., υ), FO filters exhibit amplitude, delay, and transient characteristics, which are not possible to achieve using the classical ones [2, 11]. Generalization of integer-order filters to the FO-domain allows the exact order (typically, a real number) to be realized; thereby, providing precise roll-off and strict matching of design specifications [9]. Implementations of analog FO filters involve the fractance devices (e.g., FO capacitor/inductor) [4], whose immittance relationship is

$$ I(s) = k s^{\beta}, \tag{2} $$

where in the case of FO capacitor, it is appropriate to consider $I(s)$ as an admittance and k is the pseudo-capacitance expressed in Farad/second$^{1-\beta}$. In the case of FO inductor, $I(s)$ can be considered as an impedance and k is the pseudo-inductance expressed in Henry/second$^{1-\beta}$. In both these cases, it holds $\beta \in (0, 1)$. The frequency-domain expression for s^{β} is given by $(j\omega)^{\beta} = \omega^{\beta} \angle(\beta\pi/2)$, where the analog frequency variable ω is expressed in radians per second (rad/s). Various approaches have been reported to emulate the frequency response of s^{β}, [5].

The squared magnitude function of the normalized FO Butterworth filter (FOBF) [3] is given by

$$ H_B(s) H_B(-s)|_{s=j\omega} = |H_B(j\omega)|^2 = \frac{1}{1+\omega^{2M}}, \tag{3} $$

where $M = N + \alpha$, $N \in Z^+$ and $\alpha \in (0, 1)$.

In the literature, two different approaches are reported to approximate the magnitude-frequency characteristic of the FOBF. The first technique involves mod-

eling in the complex s-plane using the FO [3, 10, 25] or the integer-order transfer functions (see [16] and the references cited therein). Alternatively, FOBFs were also designed in the complex W-plane ($W = s^{1/q}$, where $\alpha = r/q$; $r, q \in Z^+$) using the pole-placement algorithms [1, 18].

A recent work has demonstrated the effectiveness of the F-domain-based approach in the reduced order modeling of FO commensurate system [17]. While realizing FO filters with optimization techniques exist in the literature [10, 16, 25], this paper is the first attempt to design the analog FOBF directly in the complex F-plane optimally. A constrained optimization strategy is formulated to guarantee design stability. Relative to the existing W-plane based techniques [1, 18], the proposed method provides the following contributions:

1. Unlike [1], the symmetric distribution of coefficients in the denominator polynomial for the integer-order Butterworth filter is also exhibited by the proposed FOBF,
2. Higher-order FOBFs are practically realized in [1] by cascading Nth-order Butterworth filter with an αth-order one. In contrast, the proposed approach can directly generate the optimal FOBF model for any value of M,
3. Unlike [18], the all-pole structure of the Mth-order proposed model always requires N+2 terms, which is the same as that of the (N+1)th order Butterworth filter, and
4. Although the W-plane-based techniques [1, 18] generate a stable design, these methods do not provide optimal pole placement in the W-plane. Consequently, the retro-fitted model in the s-plane is also not an optimal one. In contrast, the proposed constrained optimization approach guarantees both stability as well as optimal placement of poles in the unit circle of the complex F-plane for the normalized FOBF approximant. The corresponding s-domain-based proposed model achieves lower error as compared to the cited literature in approximating the theoretical magnitude response.

In the rest of the paper, Sect. 2 presents the proposed scheme; stability and modeling performances are analyzed in Sect. 3. Experimental results are presented in Sect. 4. Finally, conclusions are drawn in Sect. 5.

2 Proposed technique

It is well-known that for a function $F = s^{\beta}$, where $\beta \in (0, 1)$, the region of instability in the s-plane ($|\theta_S| < 0.5\pi$) is mapped into $|\theta_F| < 0.5\beta\pi$ in the complex F-plane [21]. Therefore, the region of stability in the F-plane is given by $|\theta_F| > 0.5\beta\pi$.

Since $s = F^{1/\beta}$, then the squared magnitude function in the F-plane for the FOBF (normalized) can be obtained by substituting $\omega = F^{1/\beta}/j$ in (3), as represented by

$$H_B(F^{1/\beta})H_B(-F^{1/\beta}) = \frac{1}{1+\left[\left(\frac{F^{1/\beta}}{j}\right)^2\right]^M} = \frac{1}{1+(-F^{2/\beta})^M} = \frac{1}{1+(-1)^M F^{2M/\beta}}. \quad (4)$$

Selecting $\beta = M/(N+1)$ and substituting in (4) leads to the magnitude function as given below.

$$H_B(F^{1/\beta})H_B(-F^{1/\beta}) = \frac{1}{1+(-1)^M F^{2(N+1)}}. \tag{5}$$

Thus, the F-domain-based M^{th}-order Butterworth filter (normalized) is modeled as an all-pole polynomial function in F, as given by

$$H(F) = \frac{1}{D(F)} = \frac{1}{F^{N+1} + u_1 F^N + u_2 F^{N-1} + \cdots + u_2 F^2 + u_1 F + 1}, \tag{6}$$

where u_k ($k = 1, 2, \ldots$) denotes the coefficients of $D(F)$. Recall that the classical P^{th}-order ($P = 1, 2, \ldots$) Butterworth filter has an analogous representation in the s-domain [24], as given by

$$H_P(s) = \frac{1}{s^P + a_1 s^{P-1} + a_2 s^{P-2} + \cdots + a_2 s^2 + a_1 s + 1}. \tag{7}$$

The objective function for the constrained optimization problem to achieve a stable FOBF model in the F-plane is formulated as

$$f = \sum_{i=1}^{L} \left| 20\log_{10}\left|H_B(F^{1/\beta}, \omega_i)H_B(-F^{1/\beta}, \omega_i)\right| - 20\log_{10}\left|H^2(F, \omega_i, X)\right| \right|, \tag{8}$$

$$\text{Subject to: } \left|\theta_{D(F)}\right| > \theta_C,$$

where the frequency variable ω is varied with logarithmic spacing for $L = 100$ sample points between $10^{-2} - 10^2$ rad/s; $\theta_C = 0.5\beta\pi$ denotes the critical phase (in rad); $\left|\theta_{D(F)}\right|$ represents the minimum absolute phase of the roots of $D(F)$; and the decision variables vector is given by

$$X = \begin{cases} [u_1 u_2 \cdots u_{N/2}], \ N\text{: } Even \\ [u_1 u_2 \cdots u_{(N+1)/2}]. \ N\text{: } Odd. \end{cases} \tag{9}$$

Thus, the dimension (d) of the problem is $N/2$ for even values of N and $(N+1)/2$ if N is an odd number. To maintain conformity with the classical Butterworth filter, the lower bound of X is set as 0 and the upper bound (Ub) is chosen as the values of the coefficients for the P^{th}-order Butterworth filter, where $P = N + 1$, as given by

$$Ub = \begin{cases} [a_1 a_2 \cdots a_{N/2}], \ N\text{: } Even \\ [a_1 a_2 \cdots a_{(N+1)/2}]. \ N\text{: } Odd. \end{cases} \tag{10}$$

Finally, the s-domain transfer function of the proposed FOBF (normalized) can be obtained as

$$H(s) = \frac{1}{s^{(N+1)\beta} + u_1 s^{N\beta} + u_2 s^{(N-1)\beta} + \cdots + u_2 s^{2\beta} + u_1 s^{\beta} + 1}. \tag{11}$$

Table 1 Decision variables vector and pole locations of the proposed FOBFs

M	X	Roots of $D(F)$
1.5	[0.6400]	-0.3200 ± 0.9474i
2.5	[1.2325]	-1, -0.1162 ± 0.9932i
2.8	[1.7030]	-1, -0.3515 ± 0.9362i
3.2	[1.2068 2.2975]	-0.1727 ± 0.9850i, -0.4307 ± 0.9025i
3.6	[2.0929 2.5454]	-0.1525 ± 0.9883i, -0.8939 ± 0.4482i
4.2	[1.8412 2.8654]	-1, -0.4057 ± 0.9140i, -0.0149 ± 0.9999i

3 Performance analysis using MATLAB simulations

The applicability of metaheuristic algorithms for solving constrained optimization problems is well established in the literature [14]. The search process of these algorithms involves a combination of stochastic and deterministic rules. These methods employ multiple agents that explore the hyper-dimensional problem search space in the initial stages, followed by local search in the later stages. This is unlike the 'fminsearch' function in MATLAB employed in [25], where the unconstrained optimization technique involves a direct search strategy based on the Nelder–Mead simplex algorithm. The iterative nature of the metaheuristic search process may lead to higher computational time as compared to the traditional optimization algorithms. It is worth noting that metaheuristic algorithms can only achieve a near-global optimal solution. Furthermore, a closed-form solution is also not attained by a metaheuristic technique. However, these methods have established a niche due to their ease of implementation and ability to effectively handle linear or non-linear, convex or non-convex, multimodal, multidimensional, unconstrained, and constrained optimization problems.

The proposed optimization technique is implemented in MATLAB using the constrained composite differential evolution (C^2oDE) algorithm [27]. C^2oDE has demonstrated effective performance in solving the benchmark optimization problems provided in IEEE CEC2006 and CEC2010 test suites. In this work, the basic parameters for C^2oDE are set as population size = 100 and termination condition = $10000d$ function evaluations, while the internal parameters are the same as specified in [27]. The accuracy and stability of the proposed FOBFs are investigated by considering various design orders. Table 1 presents the optimal value of X obtained for design cases such as M = 1.5, 2.5, 2.8, 3.2, 3.6, and 4.2. The following observations can be made about the pole locations and stability of the designed FOBFs based on the results shown in Table 2:

1. The roots of $D(F)$ exhibit a magnitude of 1, which implies that all the poles of the proposed FOBF reside on the unit circle in the F-plane. A comparable situation exists for the pole locations of the classical Butterworth filter (normalized), where the poles are located on the unit circle in the left-half s-plane [24].
2. The region of stability in the F-plane is larger than in the s-plane for $\beta < 1$. All the proposed models achieve stability in the F-plane since all the poles of $H(F)$ have a negative real part. Note also from Table 2 that $\left|\theta_{D(F)}\right| > \theta_C$ for all the

Table 2 Phase of the roots of $D(F)$, critical phase and minimum absolute phase angle of the roots of the proposed FOBFs

M	$\angle$ Roots of $D(F)$	θ_C (°)	$\lvert\theta_{D(F)}\rvert$ (°)
1.5	±108.66°	67.50	108.66
2.5	±96.67°, 180°	74.97	96.67
2.8	±110.58°, 180°	83.98	110.58
3.2	±99.94°, ±115.51°	72.00	99.94
3.6	±98.77°, ±153.37°	81.00	98.77
4.2	±90.85°, ±113.93°, 180°	75.60	90.85

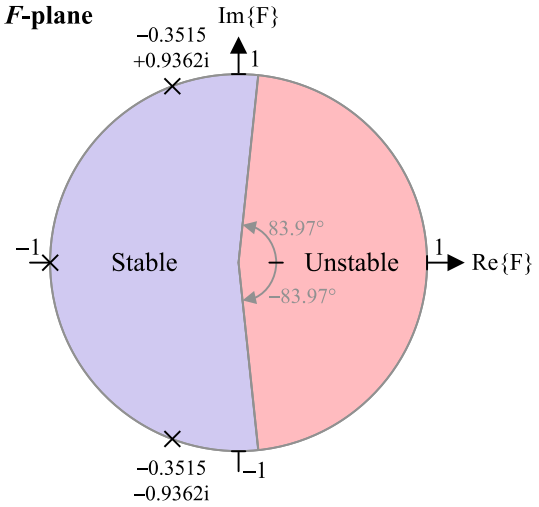

Fig. 1 Locations of poles in the F-plane for the proposed 2.8th-order Butterworth filter

cases, which further confirms the attainment of stability criteria in the F-domain for all the proposed FOBFs.

3. For odd values of N, the poles of $H(F)$ exist in complex conjugate form, whereas, for even values of N, a pole also resides at $F = -1$. As a representative, the locations of poles in the F-plane for the proposed 2.8^{th}-order Butterworth filter are presented in Fig. 1.

Table 3 shows the proposed models after transformation from F-domain to the s-domain. If M is an irrational number or it leads to the occurrence of a recurring decimal for β, then β may be truncated to three digits after the decimal point (viz., $H(s)$ for $M = 2.5, 2.8$).

The absolute relative magnitude error (ARME) metric, as defined below, is used to evaluate the modeling accuracy.

$$\text{ARME} = \left| \frac{|H(j\omega)| - |H_B(j\omega)|}{|H_B(j\omega)|} \right|. \tag{12}$$

Table 3 s-Domain transfer function of the proposed FOBFs

M	$H(s)$
1.5	$\frac{1}{s^{1.5}+0.6400s^{0.75}+1}$
2.5	$\frac{1}{s^{2.5}+1.2325s^{1.666}+1.2325s^{0.833}+1}$
2.8	$\frac{1}{s^{2.8}+1.7030s^{1.866}+1.7030s^{0.933}+1}$
3.2	$\frac{1}{s^{3.2}+1.2068s^{2.4}+2.2975s^{1.6}+1.2068s^{0.8}+1}$
3.6	$\frac{1}{s^{3.6}+2.0929s^{2.7}+2.5454s^{1.8}+2.0929s^{0.9}+1}$
4.2	$\frac{1}{s^{4.2}+1.8412s^{3.36}+2.8654s^{2.52}+2.8654s^{1.68}+1.8412s^{0.84}+1}$

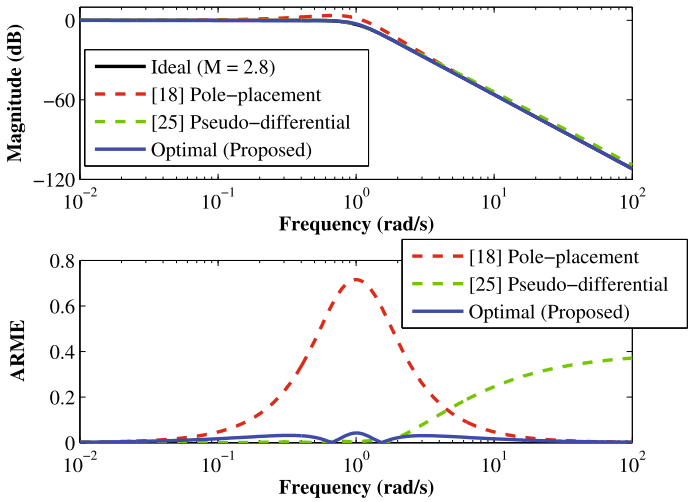

Fig. 2 Comparison of magnitude and ARME responses with the FOBFs published in the literature for 2.8^{th}-order Butterworth filter

Figure 2 (top) shows the magnitude response comparison of the proposed 2.8th-order Butterworth filter with the corresponding model published in [18, 25]. The reported model in [18] exhibits peaking near the cut-off frequency, whereas the roll-off behavior of the FOBF in [25] deviates from the theoretical one. These findings are further confirmed from the ARME comparison plots presented in Fig. 2 (bottom). The magnitude response of the proposed 3.2th-order Butterworth filter is compared with that of the published literature [18], as shown in Fig. 3. The reported design exhibits peaking in the magnitude response near the normalized cut-off frequency, whereas, the proposed model stays in proximity to the theoretical characteristic throughout the design range.

The maximum (max) and mean (evaluated using 1000 sampled frequency points with logarithmic spacing in the interval $[10^{-3}, 10^{3}]$ rad/s) ARME comparisons with

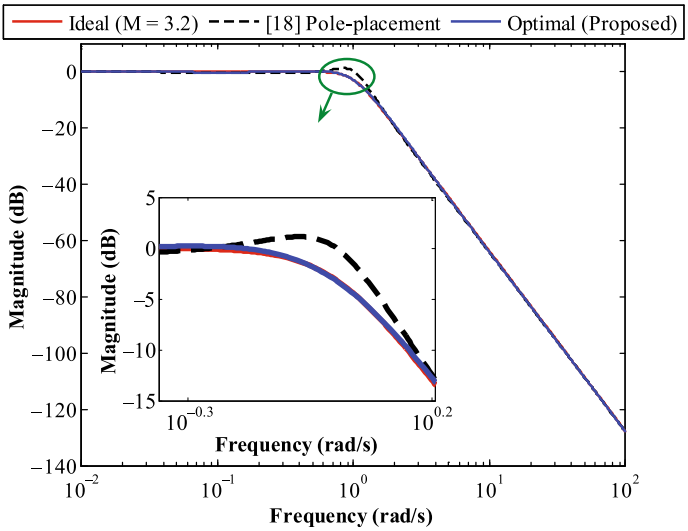

Fig. 3 Comparison of magnitude responses with the FOBF published in [18] for the 3.2th-order Butterworth filter

Table 4 Maximum and mean ARME comparisons with the FOBFs reported in the recent literature

M	FOBF Model	Max ARME	Mean ARME
1.5	[18] Pole-placement	0.07590	0.02862
	Optimal (Present work)	0.03293	0.01402
2.5	[18] Pole-placement	0.30990	0.05870
	[25] Pseudo-differential	0.95980	0.25870
	Optimal (Present work)	0.18770	0.02644
2.8	[18] Pole-placement	0.71540	0.10870
	[25] Pseudo-differential	0.39190	0.13560
	Optimal (Present work)	0.04280	0.01105
3.2	[18] Pole-placement	0.43650	0.04131
	Optimal (Present work)	0.03361	0.01443
3.6	[18] Pole-placement	0.15120	0.03979
	Optimal (Present work)	0.08938	0.02435
4.2	[18] Pole-placement	0.42250	0.06142
	Optimal (Present work)	0.29690	0.03460

the recently published literature are presented in Table 4. The proposed FOBFs achieve the least error for all the considered cases, thus demonstrating superior accuracy. The ARME comparison plots with [18] for $M = 1.5$, 2.5, 3.2, 3.6, and 4.2 are presented in Fig. 4 to justify the improved accuracy of the proposed approach graphically.

Further investigations are conducted by considering the design of $(2 + \alpha)$-order Butterworth filter with α varying from 0.01 to 0.99 in steps of 0.01. Results shown in

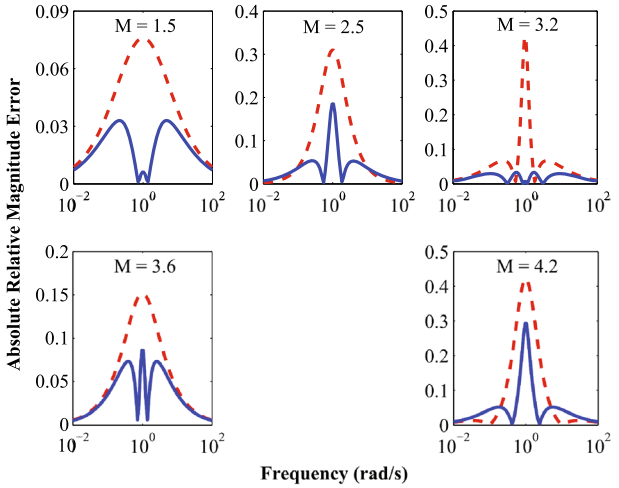

Fig. 4 ARME comparison plots between the proposed optimal FOBFs (solid blue) and the FOBFs designed using the W-plane-based pole-placement method in [18] (dashed red)

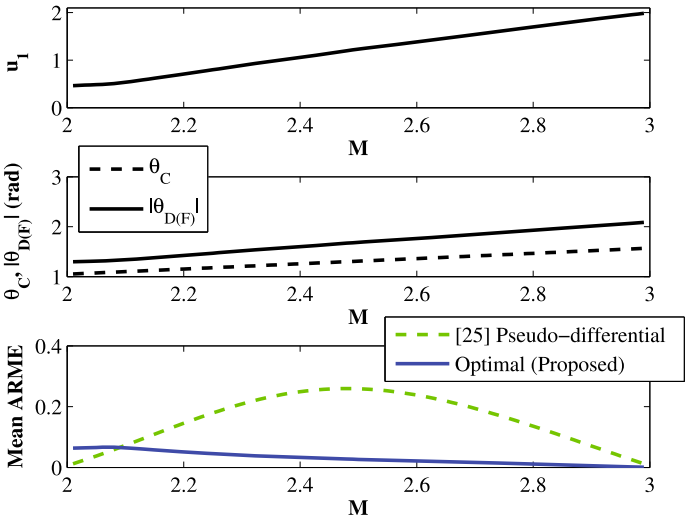

Fig. 5 Variations of u_1, θ_C, $|\theta_{D(F)}|$, and comparison with those in [25] for the proposed $(2+\alpha)$-order Butterworth filters

Fig. 5 demonstrate that: (i) coefficient u_1 increases as α is increased and u_1 approaches 2 as M approaches 3. It is noteworthy that the third-order Butterworth polynomial is given by $s^3 + 2s^2 + 2s + 1$ [24], (ii) $|\theta_{D(F)}|$ exceeds θ_C throughout the design range, which justifies the stability criterion in the F-plane for the proposed FOBFs, and (iii) the proposed designs outperform the results in [25] regarding the mean ARME for $M \in [2.10, 2.99]$.

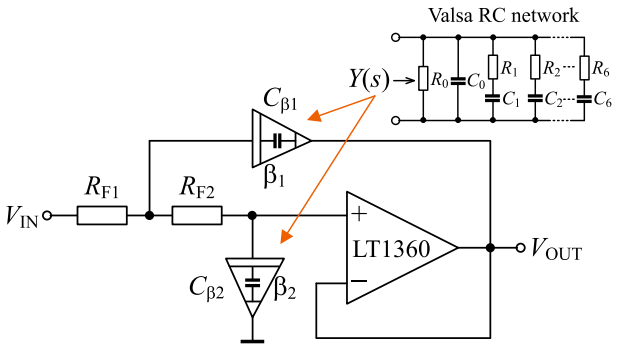

Fig. 6 Circuit realization of the proposed 1.5th order Butterworth filter using the Sallen–Key filter topology

4 Measurement results

The magnitude-frequency characteristic of the proposed 1.5th-order Butterworth filter with the transfer function as shown in Table 2 and a design cut-off frequency of 10,000 rad/s ($f_0 = 1.5915$ kHz) is verified experimentally. The filter is realized using the unity-gain Sallen–Key topology no. 1 of catalog in [22]. The operational amplifier (op-amp) based proposed circuit (see Fig. 6) employs fractional-order capacitors (FOCs) of an order $\beta = 0.75$ ($\varphi = -67.5°$) with pseudo-capacitances of $C_{\beta 1} = 100$ nF·s$^{-0.25}$ and $C_{\beta 2} = 1$ μF·s$^{-0.25}$ in place of the conventional capacitors.

A mixed-integer genetic algorithm [12], upgraded to consider parallel combinations of resistors and capacitors, was used for optimizing the phase and magnitude responses of the FOCs. The corresponding 6 branch Valsa RC ladder network-based FOC emulator [26] is also illustrated in Fig. 6. It provides a 7th-order approximation of the FOC, which has an admittance in the following general form

$$Y(s) = \frac{1}{Z(s)} = \frac{1}{R_0} + sC_0 + \sum_{k=1}^{6} \frac{sC_k}{sR_kC_k + 1}. \tag{13}$$

Electronic Industries Alliance (EIA) standard E96 (1% tolerance) and E12 (10% tolerance) compliant resistor and capacitor values, respectively, which are commercially available in 0402 size RC kits [7, 8], were used to construct the FOCs. Computed component values of the Valsa network in the desired constant phase zone (CPZ) [10^1, 10^5] Hz are listed in Table 5. The photographs of the fabricated FOC emulators with dimensions of 15 mm × 17 mm are depicted in Fig. 7. The ideal (target), simulated (nominal), and measured phase, magnitude, and pseudo-capacitance responses vs. frequency are shown in Fig. 8. Normalized histograms (%) of phase angle and pseudo-capacitance errors in the desired CPZ and the zoomed-in magnitude plot around the 10^3 Hz region are given as an inset. Simulations and Monte Carlo (MC) statistical analysis were performed in OrCAD Capture CIS 10.3 software. The MC was performed with passive element tolerances based on used datasheets for Gaussian distribution, with fixed random number seed value 17533 and 1000 runs to observe potential effects due to manufacturing processes.

Table 5 Passive element values for the fractional-order capacitors using the Valsa network

Elements	$C_{\beta 1} = 100$ nF·s$^{-0.25}$	$C_{\beta 2} = 1$ μF·s$^{-0.25}$
$R_0(\Omega)$, C_0(F)	10M ‖ 10M, 270p ‖ 1.8n	240k, 2.7n ‖ 18n
$R_1(\Omega)$, C_1(F)	1M ‖ 10M, 2.7n ‖ 15n	130k, 47n ‖ 47n
$R_2(\Omega)$, C_2(F)	30k ‖ 33k, 470p ‖ 3.3n	499 ‖ 1.21k, 3.3n ‖ 22n
$R_3(\Omega)$, C_3(F)	270k, 2.2n ‖ 6.8n	1.6k, 2.7n ‖ 39n
$R_4(\Omega)$, C_4(F)	120k ‖ 150k, 180p ‖ 5.6n	118 ‖ 130, 2.7n ‖ 15n
$R_5(\Omega)$, C_5(F)	3.6k, 560p ‖ 1.8n	12k ‖ 18k, 33n ‖ 39n
$R_6(\Omega)$, C_6(F)	1.24k ‖ 1.5k, 680p ‖ 1n	40.2k, 47n ‖ 47n

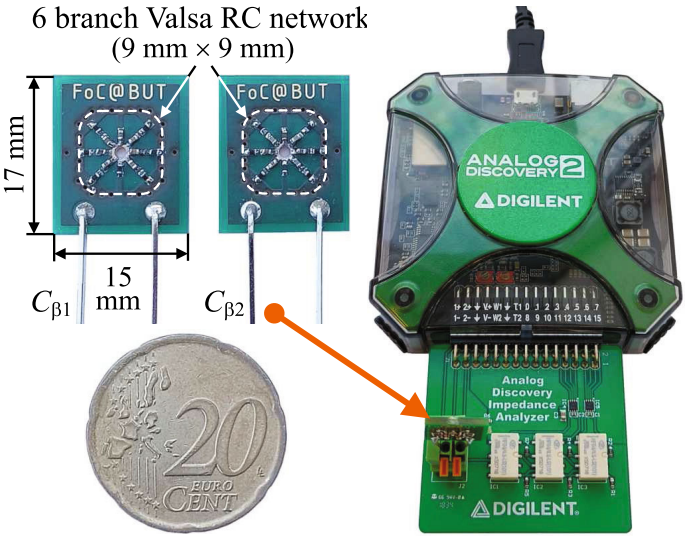

Fig. 7 Photograph of the fractional-order capacitor emulator along with the Analog Discovery 2 Impedance Analyzer

The impedance measurements were carried out using the Digilent Analog Discovery 2 device (see Fig. 7) in the frequency range of 3 Hz to 300 kHz (1001 logarithmically spaced points per five decades) with a sinusoidal input signal of 100 mV_{rms}. The performances of the FOCs in terms of relevant criteria, such as absolute phase angle deviation (APAD), phase band (PB), absolute pseudo-capacitance deviation (APCD), pseudo-capacitance band (PCB), etc., are reported in Table 6. The APAD values for the MC@1 kHz of $C_{\beta 1}/C_{\beta 2}$ are 3.123°/3.052°, respectively, while the PB metrics are ±2.554°/±2.574°. Similarly, APCD and PCB values for the MC@1 kHz are [12.480/132.879] nF·s$^{-0.25}$ and [±10.266/±124.558] nF·s$^{-0.25}$, respectively. The measured APAD values of $C_{\beta 1}/C_{\beta 2}$ are 1.035°/1.281°, respectively, while the PB metrics are yielded as ±0.622°/±0.841°. The measured APCD and PCB values are obtained as [2.123/36.029] nF·s$^{-0.25}$ and [±1.445/±16.819] nF·s$^{-0.25}$, respectively.

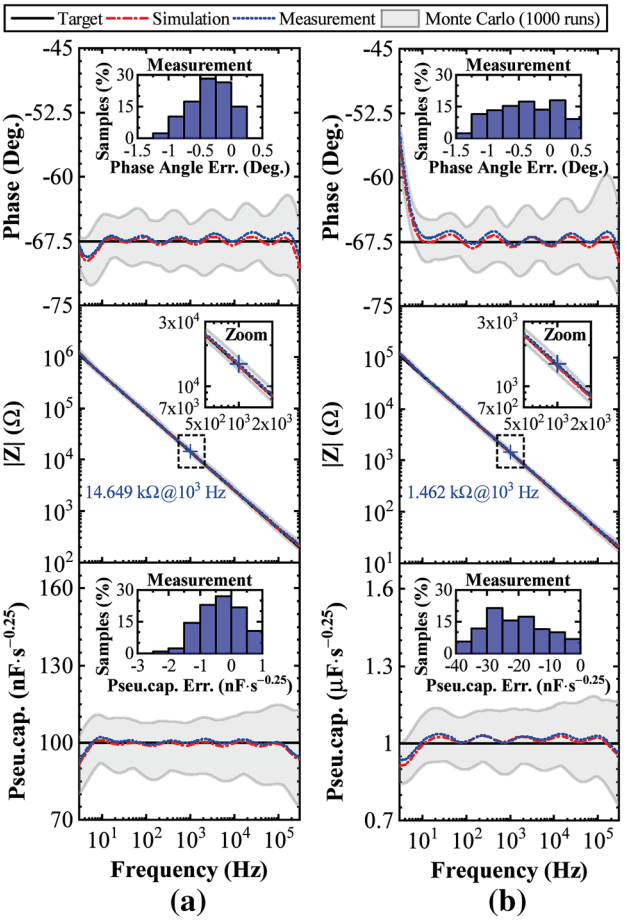

Fig. 8 Target (ideal), simulated, and measured phase, magnitude, and pseudo-capacitance-frequency responses of the 6 branch Valsa network in the frequency range of 3 Hz to 300 kHz: **a** $C_{\beta 1}$ = 100 nF·s$^{-0.25}$, **b** $C_{\beta 2}$ = 1 μF·s$^{-0.25}$. Normalized histograms (%) of phase angle and pseudo-capacitance errors in CPZ = 10 Hz to 100 kHz are shown as an inset

The comparison of measured FOC behavior with the simulated (nominal) and MC indices highlight excellent matching in the whole desired CPZ.

The proposed FOBF was assembled on a breadboard and EIA standard-compliant E96 series (1% tolerance) through-hole TESLA Lanškroun resistors (R_{F1} = 3.6 kΩ and 49.9 Ω in series, R_{F2} = 2.74 kΩ) were used. The photograph of the hardware setup is presented in Fig. 9. The supply voltage of 5 V for the op-amp LT1360 [6] was provided from the Agilent E3630A power supply. The magnitude data points for 641 logarithmic spaced frequency points in the range [10^1, 10^5] Hz were measured using the OMICRON Lab Bode 100 network analyzer and displayed using the Bode Analyzer Suite software. The level of the testing harmonic signal was set to 1.25 V_{PP}. The receiver bandwidth of the analyzer was fixed at 300 Hz. The

Table 6 Performance characteristics of the Valsa network in CPZ = 10 Hz to 100 kHz

	$C_{\beta}1 = 100\ \mathrm{nF \cdot s^{-0.25}}$			$C_{\beta 2} = 1\mu\mathrm{F \cdot s^{-0.25}}$		
Evaluation Criteria	Simulation (nominal)	Simulation (MC@1 kHz, 1000 runs)	Measurement	Simulation (nominal)	Simulation (MC@1 kHz, 1000 runs)	Measurement
Phase angle error (°)						
APAD	0.538	3.123	1.035	0.837	3.052	1.281
PB	±0.523	±2.554	±0.622	±0.798	±2.574	±0.841
Median	−0.006	0.230	−0.330	−0.019	0.556	−0.424
Mean	−0.009	0.267	−0.346	−0.042	0.545	−0.403
SD	0.303	0.791	0.311	0.464	0.874	0.480
ARME						
Max	0.01523	0.14260	0.05666	0.02951	0.13153	0.04273
Median	0.00575	0.02295	0.03141	0.01577	0.02641	0.02079
Mean	0.00642	0.02903	0.03084	0.01553	0.03076	0.02117
SD	0.00449	0.02373	0.01346	0.00789	0.02358	0.01135
Pseudo-Capacitance Error ($\mathrm{nF \cdot s^{-0.25}}$)						
APCD	1.500	12.480	2.123	30.410	132.879	36.029
PCB	±1.222	±10.266	±1.445	±18.836	±124.558	±16.819
Median	0.533	0.858	−0.351	−16.021	−9.450	−21.388
Mean	0.529	1.024	−0.354	−15.745	−10.539	−20.743
SD	0.567	3.445	0.641	8.314	38.286	9.351

APAD Absolute Phase Angle Deviation: maximum difference between a simulated/measured phase and a target one, *PB* Phase Band: the difference between a simulated/measured phase max-min error divided by two, *SD* Standard Deviation, *APCD* Absolute Pseudo-Capacitance Deviation: maximum difference between a simulated/measured C_{β} and a target one, *PCB* Pseudo-Capacitance Band: the difference between a simulated/measured C_{β} max–min error divided by two

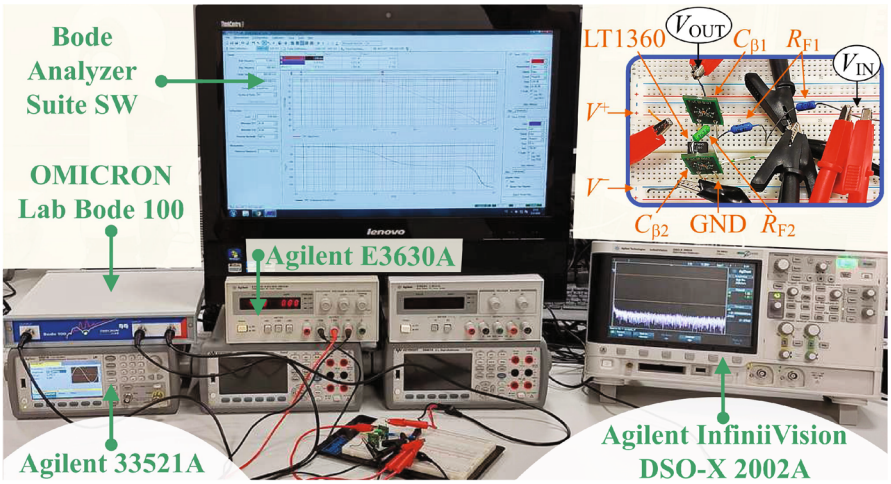

Fig. 9 Photograph of the experimental set-up to validate the proposed FOBF

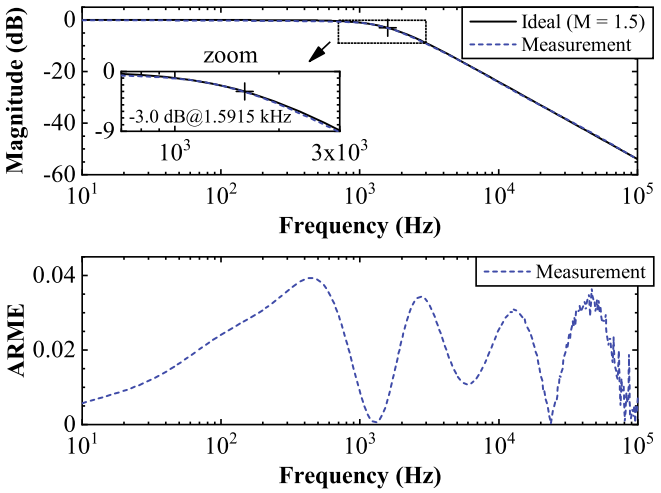

Fig. 10 Measured magnitude-frequency characteristic and ARME response of the proposed 1.5th-order Butterworth filter

time-domain behavior of the filter was observed on Agilent InfiniiVision DSO-X 2002A digital storage oscilloscope. A peak-to-peak sinusoidal voltage (V_{PP}) of 1.25 V was applied to the filter circuit from the Agilent 33521A function/arbitrary waveform generator.

The magnitude-frequency response measurement of the proposed Sallen–Key filter is compared with the ideal characteristic in Fig. 10 (top). It may be observed that the magnitude response of the practical filter conforms with the ideal behavior for the considered bandwidth. From the zoomed-in plot, it is confirmed that the magnitude of the proposed implementation at f_0 also stays in proximity with the theoretical

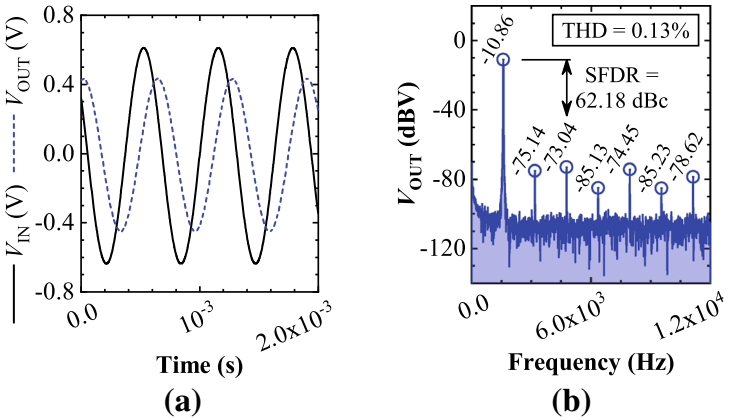

Fig. 11 Experimental **a** input–output waveforms observed in an oscilloscope and **b** Fast Fourier Transform spectrum for the proposed 1.5th order Butterworth filter with an input frequency of f_H = 1.59 kHz

value (−3.0 dB). The ARME response of the constructed filter is presented in Fig. 10 (bottom). The mean ARME value is obtained as 0.02051, whereas the max ARME of 0.03929 occurs at 434 Hz.

The time-domain response of the practical filter circuit is measured at the half-power frequency $f_H = 1.59$ kHz, as shown in Fig. 11a. For the applied V_{PP} of 1.25 V, the peak-to-peak output voltage at f_H was obtained as 0.88 V, which attains an excellent agreement with the theoretical anticipation of 0.88375 V. The Fourier spectrum of the measured output signal displayed up to the seventh harmonic is shown in Fig. 11b. Achieving a large Spurious-Free Dynamic Range (SFDR) and a small Total Harmonic Distortion (THD) for a practical filter circuit is desirable. The SFDR and the THD, evaluated from the plotted harmonics, are obtained as 62.18 dBc and 0.13%, respectively, which justifies the effectiveness of the proposed implementation.

5 Conclusions

An F-plane-based constrained optimization approach is presented for the first time to design the FOBF with guaranteed stability. Similarities with the classical Butterworth low-pass filter and advantages over the W-plane-based FOBFs are highlighted. Superior accuracy over the recent literature about the maximum and mean ARME is demonstrated through several examples. The proposed FOBF of order 1.5 was realized using the Sallen–Key filter employing fractional-order capacitor emulators. Experimental results exemplified an excellent agreement with the theoretical magnitude response. However, the proposed metaheuristic optimization approach based on C^2oDE algorithm has two limitations: (i) it does not guarantee the generation of global optimal solution, and (ii) a closed-form solution is not attainable. Further research from both the optimization and the fractional calculus community is needed to alleviate these limitations.

Acknowledgements This article is based upon work from COST Action CA15225, a network supported by COST (European Cooperation in Science and Technology).

Declarations

Conflict of interest The authors declare that they have no conflict of interest.

References

1. Acharya, A., Das, S., Pan, I., Das, S.: Extending the concept of analog Butterworth filter for fractional order systems. Signal Process. **94**, 409–420 (2014). https://doi.org/10.1016/j.sigpro.2013.07.012
2. Adhikary, A., Sen, S., Biswas, K.: Practical realization of tunable fractional order parallel resonator and fractional order filters. IEEE Trans. Circ. Syst. I **63**(8), 1142–1151 (2016). https://doi.org/10.1109/TCSI.2016.2568262
3. Ali, A.S., Radwan, A.G., Soliman, A.M.: Fractional order Butterworth filter: active and passive realizations. EEE J. Emerg. Sel. Top. Circ. Syst. **3**(3), 346–354 (2013). https://doi.org/10.1109/JETCAS.2013.2266753
4. Biswas, K., Bohannan, G., Caponetto, R., Lopes, A.M., Machado, J.A.T.: Fractional-Order Devices. Springer International Publishing, Cham (2017)
5. Colín-Cervantes, J.D., Sánchez-López, C., Ochoa-Montiel, R., Torres-Muñoz, D., Hernández-Mejía, C.M., Sánchez-Gaspariano, L.A., González-Hernández, H.G.: Rational approximations of arbitrary order: a survey. Fractal Fract. **5**(4), 267 (2021). https://doi.org/10.3390/fractalfract5040267
6. Datasheet: Linear Technology Corporation 'LT1360 50MHz, 800V/μs Op Amp'. Document no. 1360fa LT/TP 0400 2K REV A. (1994). https://tinyurl.com/LT1360
7. Datasheet: Vishay Intertechnology, Inc. 'Surface Mount Multilayer Ceramic Chip Capacitors for Commercial Applications VJ0402 X7R 10% Kit'. Document no. 45199, rev. (2019). https://tinyurl.com/VISHAY-C0402
8. Datasheet: YAGEO Corporation 'General Purpose Chip Resistors RC_L series RC0402FR-SKE96L 1R-10M 1% Kit'. Document no. May 15, 2020 V.11. https://tinyurl.com/YAGEO-R0402
9. Elwakil, A.S.: Fractional-order circuits and systems: an emerging interdisciplinary research area. IEEE Circ. Syst. Magn. **10**, 40–50 (2010). https://doi.org/10.1109/MCAS.2010.938637
10. Freeborn, T.J.: Comparison of $(1+\alpha)$ fractional-order transfer functions to approximate low pass Butterworth magnitude responses. Circ. Syst. Signal Process. **35**(6), 1983–2002 (2016). https://doi.org/10.1007/s00034-015-0226-y
11. Helie, T.: Simulation of fractional-order low-pass filters. IEEE/ACM Trans. Audio Speech Lang. Process. **22**(11), 1636–1647 (2014). https://doi.org/10.1109/TASLP.2014.2323715
12. Kartci, A., Agambayev, A., Farhat, M., Herencsar, N., Brancik, L., Bagci, H., Salama, K.N.: Synthesis and optimization of fractional-order elements using a genetic algorithm. IEEE Access **7**, 80233–80246 (2019). https://doi.org/10.1109/ACCESS.2019.2923166
13. Kilbas, A.A., Srivastava, H.M., Trujillo, J.J.: Theory and Applications of Fractional Differential Equations. Elsevier, Amsterdam (2006)
14. Kulkarni, A.J., Mezura-Montes, E., Wang, Y., Gandomi, A.H., Krishnasamy, G. (eds.): Constraint Handling in Metaheuristics and Applications. Springer, Singapore (2021)
15. Machado, J.A.T., Kiryakova, V.: The chronicles of fractional calculus. Fract. Calc. Appl. Anal. **20**(2), 307–336 (2017). https://doi.org/10.1515/fca-2017-0017

16. Mahata, S., Herencsar, N., Kubanek, D.: Optimal approximation of fractional-order Butterworth filter based on weighted sum of classical Butterworth filters. IEEE Access **9**, 81097–81114 (2021). https://doi.org/10.1109/ACCESS.2021.3085515
17. Mahata, S., Herencsar, N., Alagoz, B.B., Yeroglu, C.: Optimal F-domain stabilization technique for reduction of commensurate fractional-order SISO systems. Fract. Calc. Appl. Anal. **25**(2), 803–821 (2022). https://doi.org/10.1007/s13540-022-00014-6
18. Mishra, S.K., Upadhyay, D.K., Gupta, M.: Approximation of fractional-order Butterworth filter using pole-placement in W-plane. IEEE Trans. Circ. Syst. II **68**(10), 3229–3233 (2021). https://doi.org/10.1109/TCSII.2021.3074076
19. Mohapatra, A.S., Biswas, K.: A fractional order notch filter to compensate the attenuation-loss due to change in order of the circuit. IEEE Trans. Circ. Syst. I **68**(2), 655–666 (2021). https://doi.org/10.1109/TCSI.2020.3038282
20. Podlubny, I.: Fractional Differential Equations. Academic Press, San Diego (1999)
21. Radwan, A.G., Soliman, A.M., Elwakil, A.S., Sedeek, A.: On the stability of linear systems with fractional-order elements. Chaos **40**, 2317–2328 (2009). https://doi.org/10.1016/j.chaos.2007.10.033
22. Sallen, R.P., Key, E.L.: A practical method of designing RC active filters. IRE Trans. Circ. Theory **2**(1), 74–85 (1955). https://doi.org/10.1109/TCT.1955.6500159
23. Samko, S.G., Kilbas, A.A., Marichev, O.I.: Fractional Integrals and Derivatives Theory and Applications. Gordon and Breach Science Publishers, Amsterdam (1993)
24. Schaumann, R., Van Valkenburg, M.E.: Design of Analog Filters. Oxford University Press, New York (2001)
25. Sladok, O., Koton, J., Kubanek, D., Dvorak, J., Psychalinos, C.: Pseudo-differential $(2+\alpha)$-order Butterworth frequency filter. IEEE Access **9**, 92178–92188 (2021). https://doi.org/10.1109/ACCESS.2021.3091544
26. Valsa, J., Vlach, J.: RC models of a constant phase element. Int. J. Circ. Theory Appl. **41**(1), 59–67 (2013). https://doi.org/10.1002/cta.785
27. Wang, B.C., Li, H.X., Li, J.P., Wang, Y.: Composite differential evolution for constrained evolutionary optimization. IEEE Trans. Syst. Man Cybern. Syst. **49**(7), 1482–1495 (2019). https://doi.org/10.1109/TSMC.2018.2807785